Inversion Algorithm for Microwave Breast Cancer Detection Using Level Sets

N. Irishina, D. Álvarez, O. Dorn, P. Medina, and M. Moscoso
University Carlos III de Madrid, Spain

Abstract— This work focuses on the application of breast cancer detection from microwave data. We present a novel shape-based reconstruction algorithm that makes use of level set techniques. Our reconstruction algorithm consists of several stages of increasing complexity in which more details of the anatomical structure of the breast interior are incorporated successively. In particular, the algorithm approximates first the fibroglandular and fatty regions, and then determines the presence and characteristics of the tumor, such as its size and dielectric properties. The shape-based approach implies an implicit regularization of the inverse problem that creates the images, in the form of prior knowledge regarding the types of tissues present in the breast. This reduces the dimensionality of the inverse problem helping to stabilize the reconstruction process. In addition, it provides well defined interfaces between the tissues. Our results demostrate the potential and feasibility of this approach to detect, locate, and characterize tumors in their early stages of development.

1. INTRODUCTION

Lately, there has been increased interest in the use of microwaves for the early detection of breast cancer. The high contrast of electromagnetic parameters of malignant tissue with respect to healthy tissue makes this technique a very promising alternative to the more traditional technique of X-ray imaging which suffers from low contrast images and a potential health risk due to the ionizing nature of the probing radiation.

Despite of the relative simplicity of the microwave imaging technique, there is still many difficulties to overcome. This is at least due in part to the high level of heterogeneity of breast tissue which is composed, among others, of fibroglandular and fatty tissues giving rise to complicated internal structures. These two type of tissue have very different dielectric properties [1, 2] that lead to significant clutter. Imaging in clutter with broadband array imaging techniques that synthetically focus the recorded signals at each point of the domain (see [3], and references therein) may lead to unstable images that cannot be used for practical purposes. We mention, though, that new broadband imaging techniques specially designed for imaging in noisy environments are currently under investigation [4, 5].

On the other hand, tomographic reconstruction techniques that use a 'classical' shape-based approach suffer from similar drawbacks when the data is acquired in very noisy environments, and the commonly used homogeneous interior assumption is adopted during the reconstruction. In 'classical' shape-based approaches, one assumes during the reconstruction that the dielectric properties are piecewise constant over the domain with only two possible values: one for the healthy tissue and other for the tumor [6]. In other words, the very complicated interior structure is not taken into account when inverting the data.

Figure 1(a) shows that the homogeneous interior assumption breaks down and that a more complicated algorithm is needed to detect the tumor. The top left and top right images represent the reference and reconstructed permittivity profiles, respectively. The level set function, which define the tumor shape, and a cross section through the tumor location, are shown in the bottom images.

Therefore, there are still several fundamental problems to be resolved before microwave data can be used for the early diagnosis of breast cancer in clinical situations. We belive that the current work is an attempt to provide one significant step toward this direction. Indeed, we consider MRI-derived breast models that capture the real heterogeneity, and show that a good estimate of the internal breast structure is essential prior to the detection of small tumors.

For this purpose, we present a four stage algorithm where we also invert for the internal structure of the breast [7]. In our algorithm, the complexity of the permittivity map increases at each new stage of the algorithm, until arriving at the complete breast model. In this way, we incorporate

our findings to the subsequent stages in the form of prior knowledge about the internal structure. In other words, we use submodels of increasing complexity at each new stage of the reconstruction process, so that the result of each preceding stage is used as the starting guess for the next one. Therefore, at each new stage, the reconstructed breast model is more refined and contains more details than the previous one.

Figure 1(b) shows the result of our reconstruction algorithm applied to the same data as in Fig. 1(a). It is apparent that with our new strategy the tumor has been detected reliably, its location has been estimated correctly, and its size and permittivity value have been approximated well. The arragement of this figure is similar to the one in Fig. 1(a).

It is important to note that in this work the shape of the fibroglandular and fatty tissues, together with their average dielectric properties are reconstructed directly from the microwave boundary data. The properties and the width of skin are assumed to be known. In references [7, 8] we assumed that, a priori, the average dielectric properties of the healthy tissue and the shape of the skin were known.

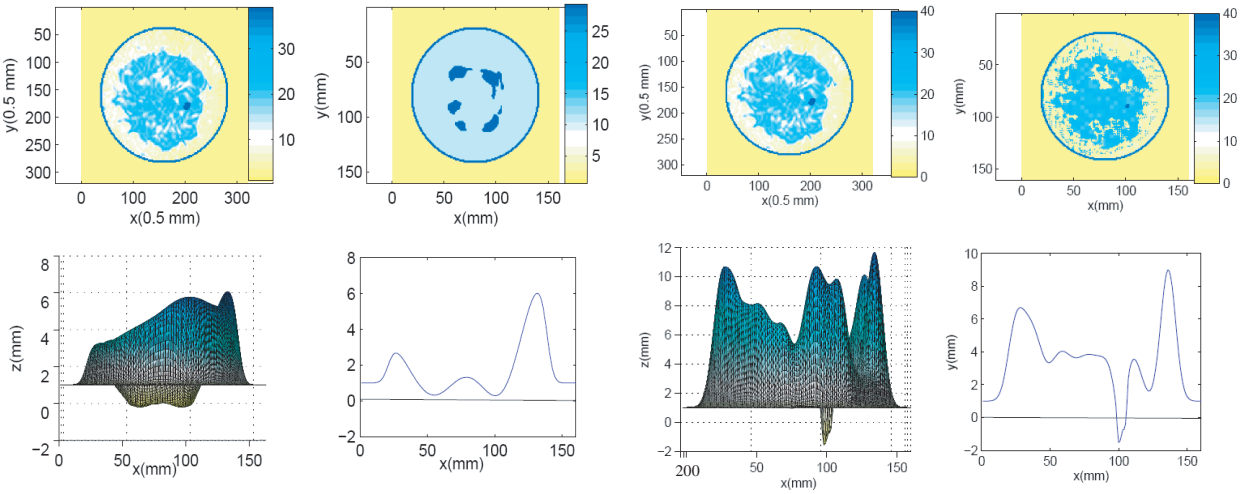

(a) Case I (b) Case II

Figure 1: Simulation results for multi frequency small tumor detection in realistic breast model, using the algorithm for simplified breast model in Case I, and the new proposed inversion algorithm in Case II. In both cases, top row: left-the static permittivity map of reference, right- the reconstruction result; bottom row: left-final level set function side view, right-cross section of the final level set function through the tumor location.

2. FORWARD MODEL

We consider a heterogeneous 2D medium Ω (see the top left images of Figs. 1(a) and (b)), illuminated by TM waves. To describe the non zero component of the electric field, we use the scalar Helmholtz equation

$$\Delta u + \kappa(\mathbf{x})u = -q(\mathbf{x}) \quad \text{in } \Omega \tag{1}$$

with $\kappa(\mathbf{x}) = \omega^2\mu_0\epsilon_0\epsilon_r^*(\mathbf{x})$, where $\epsilon_r^*(\mathbf{x})$ is the complex relative permittivity. The field u is required to satisfy the Sommerfeld radiation and is assumed to be continuous together with its normal derivatives across interfaces.

We solve Eq. (1) numerically with a second order centered finite differences scheme and a perfectly matching layer (PML) for numerically terminating the computational domain. To avoid the inverse crime we use different meshes for the 'true' data (320×320 pixels of size $0.5 \times 0.5\,\text{mm}^2$) and for the reconstruction (160×160 pixels of size $1 \times 1\,\text{mm}^2$). We use 40 antennas, situated equidistantly around the breast. The microwaves of frequencies 1–5 GHz with sampling rate of 1.0 GHz are used to define the shapes of the fibroglandular region and the tumor and their dielectrical properties.

To model the dispersion in biological tissue, we use the single pole Debye relaxation model [2],

in which the complex relative permittivity is introduced as follows:

$$\epsilon_r^* = \epsilon_\infty + \frac{\epsilon_{st} - \epsilon_\infty}{1 - i\omega\tau} + i\frac{\sigma_{st}}{\omega\epsilon_0} \ , \tag{2}$$

where ϵ_∞ is the high frequency infinite permittivity, ϵ_{st} is the low frequency static permittivity, and σ_{st} is the static conductivity, τ is the relaxation time.

With this model there are three independent parameters to be reconstructed. Motivated by the results of Table 1 in [9], we simplify our model assuming that there exits a linear relation between them. We will assume that they approximately follow the relations $\epsilon_\infty = 7.700 - 0.0677\epsilon_{st}$ and $\sigma_{st} = 0.03 + 0.01\epsilon_{st}$. Hence, in our model the only parameter to be reconstructed is ϵ_{st}. The other two parameters are given automatically by the previous relations.

For our numerical experiments we use a MRI-derived numerical breast model. The MRI pixel intensities are mapped to the Debye parameters. The average Debye parameters are arbitrary, so they are choosen from representative values published in the literature [1]. The fibroglandular and fat average static permittivity value are $\epsilon_{st}^{fiber} = 23,19$ and $\epsilon_{st}^{fat} = 8.20$. The skin layer is 1.5-mm thick with Debye parameters $\epsilon_{st}^{skin} = 37$, $\epsilon_\infty^{skin} = 4$, and $\sigma_{st}^{skin} = 1.1$ S/m. The surrounding medium has parameters $\epsilon_{liquid} = 2.6$, $\sigma_{liquid} = 0.04\,\mathrm{S/m}$. Since relaxation time is similar for different biological tissues, we set $\tau = 7.0$ ps in all tissues.

For simplicity, all the tumors have $\epsilon_\infty^{tumor} = 3.9$ and $\sigma_{st}^{tumor} = 0.7\,\mathrm{S/m}$, and their dielectric parameters are spatially independent.

3. LEVEL SET FORMULATION OF THE INVERSE PROBLEM

In the level set approach of shape reconstruction, the unknown shapes of the fibroglandular region and the tumor will be implicitly represented by two different 'level set functions' $\psi(\mathbf{x})$ and $\phi(\mathbf{x})$. We introduce two sufficiently smooth level set functions ψ and ϕ such that

$$\kappa(\mathbf{x}) \ = \ \begin{cases} \kappa_{tum}(\mathbf{x}) & \text{where} \quad \phi(\mathbf{x}) \le 0, \\ \kappa_{fib}(\mathbf{x}) & \text{where} \quad \phi(\mathbf{x}) > 0 \text{ and } \psi(\mathbf{x}) \le 0 \ , \\ \kappa_{fat}(\mathbf{x}) & \text{where} \quad \phi(\mathbf{x}) > 0 \text{ and } \psi(\mathbf{x}) > 0 \ . \end{cases} \tag{3}$$

Here, the functions κ_{fib} and κ_{fat} denote the (squared) wavenumber inside the fibroglandular and fatty tissue regions, respectively, and κ_{tum} denotes the wavenumber inside the tumor. In order to derive evolution laws for the individual unknowns, we write (3) in the alternative form

$$\kappa(\mathbf{x}) \ = \ \kappa_{tum}(1 - H(\phi)) + H(\phi)\Big[\kappa_{fib}(1 - H(\psi)) + \kappa_{fat}H(\psi)\Big] \ , \tag{4}$$

where H denotes the Heaviside step function whose value is zero for negative arguments and one for positive arguments. Here, $\kappa = \kappa(\phi, \psi, \kappa_{fib}, \kappa_{fat})$, and our goal is to reduce and eventually minimize the least squares cost functional

$$J(\kappa(\phi, \psi, \kappa_{fib}, \kappa_{fat})) \ = \ \frac{1}{2}\big\|R(\kappa(\phi, \psi, \kappa_{fib}, \kappa_{fat}))\big\|^2 \ .$$

Here, $R(\kappa)$ denotes the difference between the measured data and the calculated by the forward solver using the parameter distribution κ given by (3). Notice that we have formally not included κ_{tum} in the list of unknowns since we will treat this important parameter with a special technique in our approach as explained further below.

Let us introduce an artificial evolution time t for the above specified unknowns of the inverse problem. Then, the goal is to find evolution laws

$$\frac{d\phi}{dt} \ = \ f(t), \ \frac{d\psi}{dt} \ = \ g(t), \ \frac{d\kappa_{fib}}{dt} \ = \ h_{fib}(t), \ \frac{d\kappa_{fat}}{dt} \ = \ h_{fat}(t) \ , \tag{5}$$

such that the cost functional J decreases with time. It can be shown by straightforward formal calculation [8], that the following choices for the forcing functions point into descent directions of J:

$$\begin{aligned} f(t) \ &= \ -C_\phi(t)\mathrm{Re}\Big[R'[\kappa]^* R[\kappa]\Big(\kappa_{fib}(1 - H(\psi)) + \kappa_{fat}H(\psi) - \kappa_{tum}\Big)\Big], \\ g(t) \ &= \ -C_\psi(t)\mathrm{Re}\big[R'[\kappa]^* R[\kappa]H(\phi)\big(\kappa_{fat} - \kappa_{fib}\big)\big], \\ h_{fib}(t) \ &= \ -C_{fib}(t)\mathrm{Re}\big[R'[\kappa]^* R[\kappa]\big]H(\phi)(1 - H(\psi)), \\ h_{fat}(t) \ &= \ -C_{fat}(t)\mathrm{Re}\big[R'[\kappa]^* R[\kappa]\big]H(\phi)H(\psi) \ . \end{aligned} \tag{6}$$

In these expressions, $R'[\kappa]^*$ is the adjoint of the linearized residual operator $R'[\kappa]$, and the expression $R'[\kappa]^*R[\kappa]$ represents the Fréchet derivative of $R[\kappa]$ with respect to κ. Positive-valued constants C_ϕ, C_ψ, C_{fib} and C_{fat} steer the speed of the evolution of each component individually. These constants can also be chosen zero, in which case the corresponding quantity does not evolve.

Numerically discretizing the evolution laws by a straightforward finite difference time-discretization with time-step $\delta t^{(n)} > 0$ in step n yields the iteration rules

$$\begin{aligned} \phi^{(n+1)} &= \phi^{(n)} + \delta t^{(n)} f^{(n)}, \quad \psi^{(n+1)} = \psi^{(n)} + \delta t^{(n)} g^{(n)}, \\ \kappa_{fib}^{(n+1)} &= \kappa_{fib}^{(n)} + \delta t^{(n)} h_{fib}^{(n)}, \quad \kappa_{fat}^{(n+1)} = \kappa_{fat}^{(n)} + \delta t^{(n)} h_{fat}^{(n)}, \end{aligned} \tag{7}$$

with suitable initializations for the four quantities at the (discretized) evolution time $t^{(0)}$.

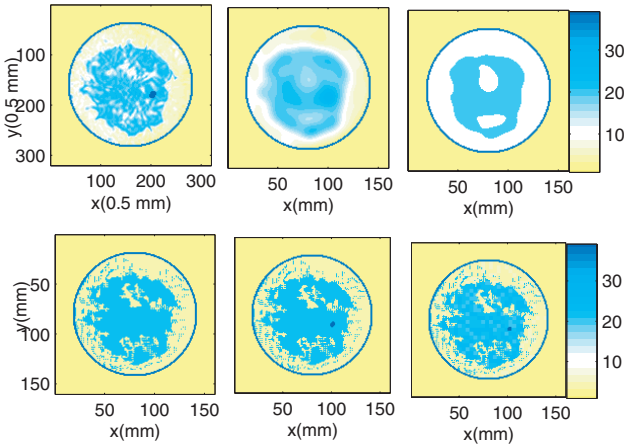

Figure 2: Top row from left to right: reference static permittivity profile, the reconstructed static permittivity map at the end of stage I, and the initial guess at the beginning of stage II. Bottom row from left to right: the reconstruction at the end of stage II, reconstruction at the end of stage III, and the final reconstruction corresponding to the minimum value of the cost functional during the IV stage.

4. INVERSION ALGORITHM FOR REALISTIC BREAST MODEL

The four stages of our algorithm are illustrated in Fig. 2. The reference permittivity profile is shown in the top left image. Hence, we start the reconstruction from and arbitrary homogeneous profile composed only of healthy tissue. We set $\phi = 1$ and $\psi = 1$ everywhere within the domain, $C_\phi = C_\psi = C_{fib} = 0$, and $C_{fat} > 0$.

The *first stage* is a pixel based reconstruction. The result at the end of this first stage is displayed in the top middle image of the figure. Note that it is very hard or even impossible to determine whether or not there is a tumor present within the breast. This is so, because pixel-based reconstruction strategies tipically oversmooth estimates of the breast profile.

The *second stage* carries out a shape-based reconstruction of the fibroglandular region. To this end, we first replace the reconstructed pixel by pixel profile by a bimodal distribution, as it is shown in the top right image of Fig. 2. Again, we only consider healthy tissue (fat and fibroglandular) in this stage, ignoring the possible presence of the tumor. Hence, we set $\phi = 1$, and $C_\phi = 0$, $C_\psi > 0$, $C_{fib} > 0$, and $C_{fat} > 0$. Starting from our initial guess (top right image), we apply our algorithm and arrive to the reconstruction shown in the bottom left image when the cost functional J does not decrease any more.

During the *third stage*, we search for the location and the shape of the tumor. We assume no initial tumor shape in this stage so, initially, $\phi = 1$. If a tumor is detected, we fix its static permittivity value to $\epsilon_{tum}^{(0)} = 35$. During this stage, $C_\phi > 0$, $C_\psi > 0$, and $C_{fib} = C_{fat} = 0$. Starting, from the reconstructed profile achieved at the end of the previous stage, we apply the algorithm and we obtain the profile shown in the bottom middle image. The result shows that the tumor has been located properly and its shape has been estimated well.

The *fourth stage* probably deals with the most difficult task: to specify the correct dielectric properties and shape of the small tumor. We now assume that the shapes and internal properties of the fatty and fibroglandular regions have already been estimated well, so we keep $(\psi, \epsilon_{fib}, \epsilon_{fat})$

fixed. Therefore, $C_\psi = C_{fib} = C_{fat} = 0$ and $C_\phi > 0$. To find the optimal values $(\phi^{opt}, \epsilon_{tum}^{opt})$ that fit the data, corresponding to the global minimum of the cost functional, we use a hybrid strategy combining a gradient technique for the shape of the tumor and a sampling strategy for its dielectric properties. At the end, we pick the reconstruction corresponding to the global minimum of J. See the resulting map in Fig. 2 bottom right image. Our algorithm is able to identify a very small tumor taking into account the high heterogeneity of the breast, and provides useful information on its size and dielectric properties.

5. CONCLUSION

Our reconstruction strategy is able to detect millimeter size tumors and simultaneously determine their locations, sizes, and permittivity values, applied to realistic MRI derived breast models. Being able to recover the dielectric properties of a detected object in the breast could help to discriminate between benign and malignant tumors, and may lead to determine whether a normal tissue is in the process of becoming malignant. Our algorithm can be used to determine the type of the internal breast structure, as well. The use of the level set technique may be important for the design of new microwave imaging systems.

REFERENCES

1. Meaney, P. M., M. W. Fanning, T. Raynolds, C. J. Fox, Q. Fang, C. A. Kogel, S. P. Poplack, and K. D. Paulsen, "Initial clinical experience with microwave breast imaging in women with normal mammography," *Acad. Radiol.*, Vol. 14, 207–218, 2007.
2. Lazebnik, M., M. Okoniewki, J. Booske, and S. Hagness, "Highly accurate debye models for normal and malignant breast tissue dielectric properties at microwave frequencies," *IEEE Microwave and Wireless Components Letters*, Vol. 17, 822–824, 2007.
3. Fear, C. E., S. C. Hagness, P. M. Meaney, M. Okoniewski, and M. A. Stuchly, "Enhancing breast tumor detection with near-field imaging," *IEEE Microwave Mag.*, 48–56, March 2002.
4. Kosmas, P. and C. Rappaport, "A matched filter FDTD-basedtime reversal approach for microwave breast cancer detection," *IEEE Trans. Antennas Propagat.*, Vol. 54, 1257–1264, 2006.
5. Borcea, L., G. Papanicolaou, and C. Tsogka, "Adaptive interferometric imaging in clutter and optimal illumination," *Inverse Problems*, Vol. 22, 1405–1436, 2006.
6. Irishina, N., M. Moscoso, and O. Dorn, "Detection of small tumors in microwave medical imaging using level sets and MUSIC," *PIERS Proceedings*, 43–47, USA, March 26–29, 2006.
7. Irishina, N., M. Moscoso, and O. Dorn, "Microwave imaging for early breast cancer detection using a shape-based strategy," *IEEE Trans. Biomed. Eng.*, in press, 2009.
8. Irishina, N., O. Dorn, and M. Moscoso, "A level set evolution strategy in microwave imaging for early breast cancer detection," *Computers and Mathematics with Applications*, Vol. 56, 607–618, 2008.
9. Winters, D. W., E. J. Bond, B. D. Van Veen, and S. C. Hagness, "Estimation of the frequency-dependent average dielectric properties of breast tissue using a time-domain inverse scatteruing techique," *IEEE Transactions on Antennas and Propagation*, Vol. 54, 3517–3528, 2006.